

Flexible and Efficient Spatio-Temporal Transformer for Sequential Visual Place Recognition

Yu Kiu (Idan) Lau, Chao Chen, Ge Jin, Chen Feng

Abstract—Sequential Visual Place Recognition (Seq-VPR) leverages transformers to capture spatio-temporal features effectively; however, existing approaches prioritize performance at the expense of flexibility and efficiency. In practice, a transformer-based Seq-VPR model should be flexible to the number of frames per sequence (seq-length), deliver fast inference, and have low memory usage to meet real-time constraints. To our knowledge, no existing transformer-based Seq-VPR method achieves both flexibility and efficiency. To address this gap, we propose Adapt-STformer, a Seq-VPR method built around our novel Recurrent Deformable Transformer Encoder (Recurrent-DTE), which uses an iterative recurrent mechanism to fuse information from multiple sequential frames. This design naturally supports variable seq-lengths, fast inference, and low memory usage. Experiments on the Nordland, Oxford, and NuScenes datasets show that Adapt-STformer boosts recall by up to 17% while reducing sequence extraction time by 36% and lowering memory usage by 35% compared to the second-best baseline.

I. INTRODUCTION

Sequential Visual Place Recognition (Seq-VPR) extends traditional VPR by leveraging multiple consecutive frames to construct more robust descriptors for a given location. By incorporating temporal information, Seq-VPR produces more consistent outputs, which is especially beneficial under challenging conditions such as low light or illumination changes [1, 2]. Methods for exchanging and aggregating spatial-temporal features across frames generally fall into two categories. The first type neglects complex cross-frame temporal interactions. For example, JIST collapses per-frame embeddings into a single descriptor via learnable mean pooling, without direct frame-to-frame interaction [1, 3, 4]. The second type draws inspiration from video understanding [5, 6, 7], where recent Seq-VPR methods integrate transformer modules to model both inter-frame (temporal) and intra-frame (spatial) interactions.

However, existing transformer-based Seq-VPR research prioritizes performance over flexibility and efficiency. In practice, a Seq-VPR model should be flexible with respect to the number of frames per sequence (seq-length). It should also be efficient in inference speed and memory usage to meet the real-time constraints of VPR systems. At present, we believe no existing transformer-based Seq-VPR model is both efficient and flexible. Some approaches use a standard transformer layer to learn temporal interactions after extracting spatial features. However, as each additional frame introduces more tokens, the transformer’s computation grows quadratically. STformer [8] reduces computation by limiting temporal attention to local windows across frames. While this windowing lowers costs, it is not flexible with respect

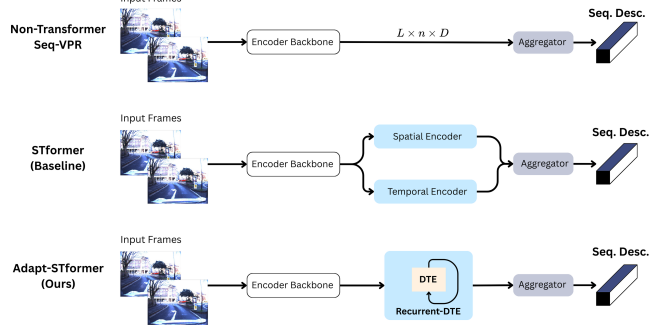


Fig. 1: Comparison of Seq-VPR architectures. Top: Non-transformer methods feed backbone features directly to an aggregator. Middle: STformer handles spatial and temporal modeling with separate encoders before aggregation. Bottom: The proposed Adapt-STformer unifies spatio-temporal modeling in the Recurrent-DTE module before aggregation.

to seq-length. This constraint reduces practical usability: when frames are missing/ distorted, the model can only rely on padding/dropping to satisfy the required seq-length. Moreover, STformer keeps separate spatial and temporal modules, adding significant overhead, leaving STformer neither flexible nor efficient.

To address this gap, we propose Adapt-STformer, a Seq-VPR framework centered on our novel Recurrent Deformable Transformer Encoder (Recurrent-DTE). Unlike prior works that process multiple frames in parallel [9, 10], our approach unifies spatio-temporal fusion within a single holistic module. The Recurrent-DTE recursively applies a lightweight Deformable Transformer Encoder (DTE) to frames in temporal order, from the earliest to the most recent. This design naturally encodes temporal dependencies, supports arbitrary seq-lengths, and achieves a favorable balance of flexibility, efficiency, and performance. We highlight the main contributions of this work as follows:

- We present Adapt-STformer, a Seq-VPR architecture that eliminates the restriction of fixed seq-length through a lightweight unified framework, thereby achieving both flexibility and efficiency. We will open source our codes upon paper acceptance.
- We introduce Recurrent-DTE, a recurrent mechanism embedded in a shared DTE that iteratively processes frames in temporal order, enabling effective spatio-temporal modeling within a unified module.
- We conduct extensive experiments on the Nordland,

Oxford, and NuScenes datasets, where Adapt-STformer achieves balanced improvements, increasing recall by 10% on average while reducing inference latency by 36% and lowering memory usage by 35%.

II. RELATED WORKS

A. Classic Seq-VPR

Early Seq-VPR methods relied on handcrafted descriptors combined across frames, but these lacked robustness to environmental changes [11]. The introduction of learning-based approaches, particularly CNN-based models, marked a shift toward data-driven sequence aggregation. SeqNet [1] applied a lightweight 1D temporal convolution to merge a sequence into a single compact descriptor. Building on this idea, SeqVLAD [3] extended NetVLAD [12] by pooling features from all frames into a unified descriptor set and applying VLAD’s soft-assignment and residual aggregation, producing a fixed-length embedding adaptable to different sequence lengths. With a focus on efficiency, JIST [4] proposed SeqGeM, a learnable mean pooling mechanism for compact sequence representation. While effective, these non-transformer Seq-VPR methods model temporal information only through simple aggregation, limiting their ability to capture complex spatio-temporal dependencies and leading to performance drops in challenging conditions [8]. Our work seeks to retain their efficiency and flexibility while addressing these limitations.

B. Transformer-based Seq-VPR

With the rise of transformers in vision tasks [6, 7], Seq-VPR methods have also adopted them to better model spatio-temporal dependencies. STFormer [8] introduced a two-stage design with a spatial transformer for frame-level features and a sliding-window temporal transformer for sequence modeling, achieving strong performance but limited by fixed sequence lengths and high computational cost due to separate encoders and dense attention. More recently, CaseVPR [13] leveraged a DINOv2 backbone [14] and correlation-aware embedding, reaching SOTA results with seq-length flexibility, but at the expense of heavy computation, slow inference, and large memory use. In short, existing transformer-based Seq-VPR methods trade flexibility and/or efficiency for performance.

C. Computationally Efficient Transformer

Deformable Transformers, proposed in [15], employ deformable attention, where each query attends to a sparse set of learned offsets, thereby reducing the quadratic cost of global self-attention on high-resolution features. Xu et al. [16] demonstrated the effectiveness of Deformable Transformer Encoders (DTE) for multi-camera VPR, although without modeling temporal features. BEVFormer [2] integrates temporal cues by recurrently fusing past BEV features and further employs a Temporal Self-Attention (TSA) layer in addition to its DTE for spatial lookup across multiple camera views. In contrast, our design unifies spatial and temporal reasoning directly within a DTE, avoiding the need for a

separate TSA layer. We found that replicating BEVFormer’s additional TSA did not improve performance and instead caused significant increases in inference time and memory usage. Beyond these architectural differences, BEVFormer assumes a synchronized multi-camera setup with known camera intrinsics. In contrast, we target a practical monocular front-view scenario without access to calibration parameters, making our method applicable to real-world settings.

D. Poor lighting VPR

BEV2PR (BEV-Enhanced Image VPR) [17] lifts monocular images into a bird’s-eye view (BEV) to explicitly model structural cues and fuse them with visual embeddings, yielding substantial gains under poor lighting. To assess our method’s capacity to leverage such structural information, we follow BEV2PR and evaluate Seq-VPR on the NuScenes dataset [18], focusing on challenging day-night conditions.

E. Computation efficient backbone

The choice of encoder backbone is crucial for our method’s performance and efficiency. Early Seq-VPR methods commonly use encoder backbones such as ResNet [19] valued for their computational efficiency but limited in representational power. In contrast, modern Vision Transformer (ViT) backbones [14, 20] offer rich, high-quality visual features learned from massive self-supervised training, yet they incur substantial computational cost. Compact Convolutional Transformer (CCT) [21] represents a hybrid of convolutional tokenization and transformer layers, showing promising performance while remaining relatively lightweight compared to pure ViT [22] counterparts. Motivated by this balance of efficiency and performance, we adopt CCT as the encoder backbone for our Seq-VPR framework.

METHODOLOGY

A. Overall Architecture

Adapt-STformer takes as input a frame sequence $S = \{s_i\}_{i=1}^L$, with each $s_i \in \mathbb{R}^{H \times W \times 3}$, and outputs a NetVLAD descriptor $V \in \mathbb{R}^{C \times D}$, where C is the number of VLAD clusters and D is the embedding dimension. There are three intermediate stages between input and output.

- **Encoder Stage:** Encode S with CCT to obtain $F = \{f_t\}_{t=1}^L \in \mathbb{R}^{L \times n \times D}$.
- **Recurrent-DTE Stage:** Refine F iteratively via Recurrent-DTE, producing $\hat{F} = \{\hat{f}_t\}_{t=1}^L \in \mathbb{R}^{L \times n \times D}$.
- **Aggregation Stage:** Aggregate \hat{F} with SeqGeM and SeqVLAD into $V \in \mathbb{R}^{C \times D}$.

B. Encoder Stage:

We adopt CCT384 as our encoder backbone to extract initial features. Given a sequence $S = \{s_i\}_{i=1}^L$ with $s_i \in \mathbb{R}^{H \times W \times 3}$, the encoder maps each frame into a tokenized feature representation. Each token is then projected into a D -dimensional feature space. The output of the encoder is therefore a tensor

$$F = \{f_t\}_{t=1}^L \in \mathbb{R}^{L \times n \times D}$$

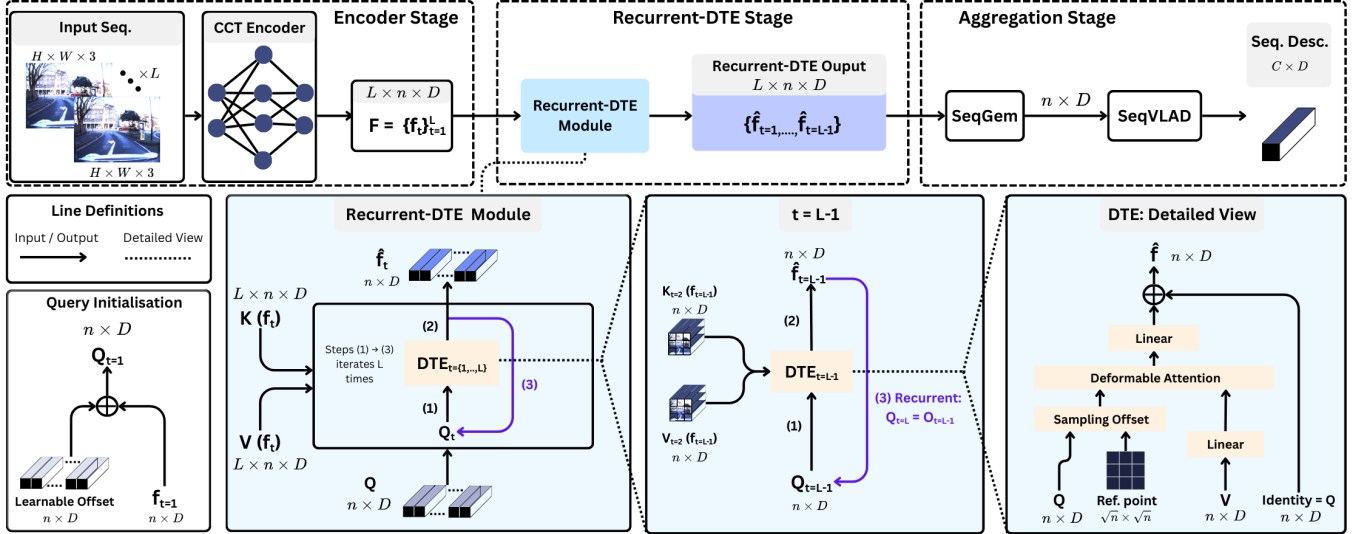


Fig. 2: **Proposed architecture of Adapt-STformer.** A frame sequence S enters the **Encoder Stage**, where the CCT384 backbone tokenizes each input frame, producing $F = \{f_t\}_{t=1}^L$. **Recurrent-DTE Stage** performs *iterative recurrent* spatio-temporal refinement on F : at iteration t , the previous DTE output provides the queries $Q_t = \hat{f}_{t-1}$ and the current frame supplies keys/values $K_t = V_t = f_t$, with $Q_{t=1} = f_{t=1} + \Delta$; this recurrence yields $\{\hat{f}_t\}_{t=1}^L$. **Aggregation Stage** stacks $\{\hat{f}_t\}$ into a tensor \hat{F} , applies SeqGeM to obtain \hat{F} , and processes it with SeqVLAD into the final sequential descriptor.

TABLE I: SUMMARY OF MAJOR NOTATIONS FOR ADAPT-STFORMER.

L	Number of frames/seq-length
t	Iteration/frame index, $t \in \{1, \dots, L\}$
f_t	The encoder output feature from the t th image
\hat{f}_t	DTE output at t
F	The set of encoder outputs across the sequence
Q_t	Query at t
K_t	Key at t
V_t	Value at t
Δ	Learnable offset

C. Recurrent-DTE Stage:

DTE: We choose DTE [15] for its deformable attention, where each query’s attention is restricted to its reference point’s neighboring keypoints. Following [15, 2], we overlay each feature map with a uniform 2D reference point grid and learn per query offsets to dynamically select sampling locations.

Recurrent-DTE: To capture temporal dependencies across frames of S , we introduce a recurrent mechanism that, at frame index t , uses the previous frame’s DTE output \hat{f}_{t-1} together with the current frame’s encoder features f_t . Here, \hat{f}_{t-1} acts as a hidden state shaped by iterations $\{0, \dots, t-1\}$. At iteration t , we set \hat{f}_{t-1} as the query Q_t and f_t as the key K_t and value V_t . Because each iteration of Recurrent-DTE relies only on the output of the previous one, the module is seq-length agnostic. For initialization, $Q_{t=1}$ is defined as the element-wise sum of $f_{t=1}$ and Δ , both of shape $n \times D$.

$$\begin{aligned} \hat{f}_t &= \text{DTE}(Q_t = \hat{f}_{t-1}, K_t = V_t = f_t) \\ Q_{t=1} &= f_{t=1} + \Delta \end{aligned} \quad (1)$$

This design differs fundamentally from [8], where tempo-

ral information is learned by a separate transformer layer. In our approach, temporal information is instead implicitly captured within the same transformer operation as spatial modeling. Recurrent-DTE therefore unifies spatio-temporal modeling within a single module.

D. Aggregation Stage

We concatenate per-iteration outputs $\{\hat{f}_{t=1}, \dots, \hat{f}_{t=L}\}$ into the tensor $\hat{F} \in \mathbb{R}^{L \times n \times D}$ and permute \hat{F} to become $\hat{F}' \in \mathbb{R}^{n \times L \times D}$ (treating tokens as the batch dimension) and apply SeqGeM [4], a learnable mean pooling over the temporal axis, collapsing L to 1:

$$\hat{F} = \text{SeqGeM}(\hat{F}') \in \mathbb{R}^{1 \times n \times D} \quad (2)$$

We then feed \hat{F} into SeqVLAD [3], which aggregates the n D -dimensional embeddings into a descriptor $V \in \mathbb{R}^{C \times D}$, where C is the number of VLAD clusters. Both SeqGeM and SeqVLAD are agnostic to the input sequence length L .

EXPERIMENT SETUP & IMPLEMENTATION DETAILS

TABLE II: DATASET DETAILS SPECIFYING THE NUMBER OF IMAGES IN THE DATABASE AND QUERY SETS.

Dataset	Split	Database / Queries
NordLand	Train set	15000 / 15000
	Test set	3000 / 3000
Oxford-Easy	Train set	3619 / 3962
	Test set	3632 / 3921
Oxford-Hard	Train set	2322 / 2585
	Test set	2970 / 2920
NuScenes	Train set	– / –
	Test set	4500 / 4000

A. Dataset

We evaluate on NordLand, Oxford RobotCar, and NuScenes datasets. Image counts are given in Table II.

NordLand: The Nordland dataset [23] comprises a collection of images captured during rail journeys across four seasons. We use the Summer-Winter pair for training, and the Spring-Fall pair for testing.

Oxford RobotCar: The Oxford RobotCar dataset [24, 25] provides large-scale urban driving sequences under diverse conditions. We construct two sub-datasets: *Oxford-Easy*, following the Oxford2 split in [8], which uses all six route sections with 2 meter frame separation; and *Oxford-Hard*, built from day-night traversals with disjoint route segments (sections 1–2 for training, 3–4 for testing) and 1 meter frame separation. Oxford-Hard is more challenging due to both route mismatch and severe lighting changes between training and test sets.

NuScenes: The NuScenes dataset [18] is a large-scale autonomous driving benchmark collected in urban environments. We select the Singapore scenes to capture urban day–night traversals under extreme lighting transitions. We split scenes into day and night and treat pairs with less than 30° of angular difference as positives, following [17]. We use Nuscenes as a test-only dataset, evaluating models trained on Oxford-Easy to assess their generalization capabilities.

B. Implementation Detail

Model hyperparameters: For the DTE, we use 8 attention heads, 8 sampling points, 2 levels (with only 1 feature level input), a dropout rate of 0.1, and 64 VLAD clusters.

Training: Following SeqVLAD [3], we initialize our CCT encoder from its authors’ pretrained weights [21] and use the ADAM optimizer [26] with a learning rate of 1×10^{-5} . Similar to [1, 3], we adopt the triplet loss from NetVLAD [12], selecting one non-trivial positive sample from descriptor space and five hardest negative samples from GNSS ground truths. During training, we set input image resolution to 384×384 , batch size to four, sequence length to five, and triplet margin to 0.1. Training stops early if Recall@5 does not improve for 5 straight epochs.

C. Baseline Seq-VPR Methods

As the choice of image encoder backbone greatly influences performance and efficiency, the main goals of Adapt-STformer, we first compare our method with four representative Seq-VPR baselines without a foundation model image encoder. Namely, we experiment with SeqNet [1], SeqVLAD [3], STformer [8], and JIST [4], applying the same training and testing procedure described above. In section II-E, we evaluate Adapt-STformer against SOTA VPR methods [20, 13]. For a fairer comparison with such methods trained on much larger datasets, we also analyze their performance under inference time constraints, which produces further insights on the value of Adapt-STformer’s efficiency.

Evaluation Criteria. Following prior work, we measure VPR performance by Recall@K, which counts a query

correct if at least one of the top-K retrieved candidates lies within 10 m for Oxford RobotCar and NuScenes, or within ± 1 frame for Nordland.

RESULTS

A. Recall comparison

We report the evaluation results of Adapt-STformer and Seq-VPR baselines in Table III. We calculate Recall@K for top K values of 1, 5, and 10 and measure the memory usage and duration of one forward pass for each model.

Nordland and Oxford-Easy: SeqVLAD, STformer, and our method achieve near-perfect recall on Nordland. This can be attributed to Nordland’s minor lighting variations between the query and the database, making it an easy dataset. On the Oxford-Easy dataset, we achieve a +3% R@1 gain over STformer. While Oxford-Easy presents more lighting challenges than Nordland, its train and test sets share overlapping locations, simplifying the task.

Oxford-Hard and NuScenes: Substantial gains are observed on harder benchmarks: Oxford-Hard (poor lighting, rain, and unseen sections) and NuScenes (poor lighting and cross-domain train-test splits). On Oxford-Hard, we achieve approximately +20% gains in R@1,5,10 over SeqVLAD. For NuScenes, we observe +10%, 17%, 17% improvements in R@1,5,10, respectively, over STformer.

PCA: For fairness, we further calculate Recall@K after reducing descriptors via PCA [27] to equal dimensionality. The relative performance ranking of the methods remains unchanged.

B. Resource Usage

Computational efficiency is critical for practical deployment of VPR systems and a central focus of our work. Table III reports the overall resource usage of all methods. In table IV, we make a per-module inference times comparison between Adapt-STformer (ours) and STformer, the most architecturally analogous baseline. All experiments were conducted using PyTorch [28] on an NVIDIA Tesla V100 GPU.

Transformer Modules: For spatially attending to a single frame, Adapt-STformer’s DTE module is 71.3% faster than the non-deformable transformer encoder in STformer. Also when spatio-temporally processing an entire query, our Recurrent-DTE architecture uses 88.1% less time than STformer’s additional temporal transformer encoder.

Aggregation Modules: While both methods employ SeqVLAD for sequence aggregation, Adapt-STformer first applies SeqGeM to collapse the aggregation input $\hat{F} \in \mathbb{R}^{L \times n \times D}$ tensor into $1 \times n \times D$, introducing negligible overhead while accelerating the subsequent SeqVLAD operation by 56.8%.

Overall Comparison: Overall, Adapt-STformer extracts descriptors 36% faster per sequence and requires 35% less memory than STformer (Table IV). It even achieves faster descriptor extraction than SeqVLAD, a non-transformer Seq-VPR method.

TABLE III

ADAPT-STFORMER (OURS) IS COMPARED WITH FOUR SEQ-VPR BASELINES IN TERMS OF RECALL, MEMORY (MB), AND INFERENCE TIME (S) PER SEQUENCE. BEST RESULTS ARE SHOWN IN **BOLD**, SECOND-BEST IN UNDERLINE. THE CHANGE IN DESCRIPTOR DIMENSIONALITY FOR THE SAME METHOD IS ACHIEVED THROUGH PCA AND THUS DOESN'T IMPACT RESOURCE USAGE.

Descriptor Dimension	Method	Backbone	NuScenes			Oxford-Hard			Oxford-Easy			Nordland			Resource Usage	
			R@1 ↑	R@5 ↑	R@10 ↑	R@1 ↑	R@5 ↑	R@10 ↑	R@1 ↑	R@5 ↑	R@10 ↑	R@1 ↑	R@5 ↑	R@10 ↑	Mem (MB) ↓	Time (s) ↓
24576	Seqvlad	CCT384	0.3236	0.4327	0.5142	0.4709	0.5601	0.6151	0.8275	0.9249	0.9541	0.9603	0.9947	<u>0.9947</u>	177.66	<u>0.0181</u>
	STformer	CCT384	<u>0.4461</u>	<u>0.5319</u>	<u>0.5945</u>	<u>0.5754*</u>	<u>0.6548*</u>	<u>0.7011*</u>	<u>0.8488</u>	<u>0.9323</u>	<u>0.9633</u>	<u>0.9697</u>	0.9947	0.9950	276.55	0.0277
	Ours	CCT384	0.5496	0.7035	0.7622	0.6940	0.7706	0.7969	0.8854	0.9528	0.9700	0.9763	<u>0.9943</u>	<u>0.9947</u>	<u>180.39</u>	0.0178
4096 (PCA)	Seqnet	NetVLAD	0.0827	0.1575	0.2031	0.3064	0.4505	0.5228	0.5363	0.7467	0.8241	0.7943	0.9013	0.9317	676.09	0.0014
	Seqvlad	CCT384	0.3236	0.4327	0.5146	0.4603	0.5550	0.6151	0.8280	0.9251	0.9557	0.9567	0.9947	<u>0.9947</u>	177.66	0.0181
	STformer	CCT384	0.4461	0.5319	0.5949	<u>0.5648*</u>	<u>0.6453*</u>	<u>0.6968*</u>	<u>0.8534</u>	<u>0.9372</u>	<u>0.9667</u>	0.9700	0.9947	0.9950	276.55	0.0277
512 (PCA)	Ours	CCT384	0.5488	0.7031	0.7622	0.6874	0.7659	0.7918	0.8882	0.9544	0.9710	<u>0.9610</u>	<u>0.9923</u>	<u>0.9937</u>	<u>180.39</u>	<u>0.0178</u>
	JIST ^{pc}	ResNet	0.2047	0.3146	0.3713	0.4423	0.5405	0.6139	0.5868	0.7416	0.8134	0.8210	0.9200	0.9450	159.65	0.0053
	Seqvlad	CCT384	0.3146	0.4236	0.5024	0.4383	0.5330	0.6049	0.8236	0.9244	0.9564	<u>0.9567</u>	0.9947	<u>0.9947</u>	<u>177.66</u>	0.0181
	STformer	CCT384	<u>0.4445</u>	<u>0.5370</u>	<u>0.5969</u>	<u>0.5377*</u>	<u>0.6198*</u>	<u>0.6720*</u>	<u>0.8513</u>	<u>0.9369</u>	<u>0.9667</u>	0.9637	<u>0.9933</u>	0.9950	276.55	0.0277
	Ours	CCT384	0.5551	0.7091	0.7717	0.6516	0.7459	0.7765	0.8870	0.9554	0.9731	0.9490	0.9900	0.9943	180.39	<u>0.0178</u>

* STformer was retrained on Oxford-Hard since the released models use a different split; results are reported for completeness but not analyzed. ^{pc} JIST is evaluated using a public checkpoint, as its original training procedure differs from ours.

TABLE IV: PER-MODULE INFERENCE TIME BREAKDOWN AND OVERALL RESOURCE USAGE COMPARISON BETWEEN OUR METHOD AND STFORMER.

Method	Inference Time (ms)				Memory ↓ (MB)
	Spatial Attn. ↓	Spatio-Temp↓	Aggr.↓	Overall↓	
STformer	1.71	23.02	3.98	27.7	276.55
Ours	0.49	2.73	1.72	17.8	180.39

Note: Our encoder backbone takes approx. 14 ms, accounting for the gap between module times and total inference time.

D. Ablation Study

We conduct ablation studies on Oxford-Hard and NuScenes to assess the effects of sequence length L and the proposed Recurrent-DTE. All models were trained on $L = 5$ and evaluated at $L = 3$ and $L = 1$, demonstrating flexibility to shorter seq-lengths under limited inference resources [29]

Sequence Lengths: As shown in Table V, performance increases with longer sequences. On Oxford-Hard, our Recurrent-DTE rises from 0.7341 ($L = 1$) to 0.7706 ($L = 5$), while on NuScenes it improves from 0.6224 to 0.7039. This demonstrates the ability of our approach to exploit additional temporal context as L grows effectively.

Spatio-Temporal Methods: Table V further compares different spatio-temporal methods. In the non-recurrent variant (DTE Only), each frame is processed independently, with $Q_t, K_t, V_t = f_t$, yielding no cross-frame interaction. Our Recurrent-DTE consistently outperforms this baseline across all sequence lengths, with gains of up to 18% (NuScenes, $L = 3$), while requiring no additional memory and only negligible runtime overhead. We also evaluate using a separate temporal transformer layer (DTE + TT), similar to [8, 13]. Although competitive on Oxford-Hard ($L = 1$: 0.7368 vs. 0.7341), this approach is substantially weaker on NuScenes ($L = 3$: 0.4764 vs. 0.6681), while being 32% slower (0.0177s vs. 0.0128s) and 12% more memory

TABLE V: ABLATION STUDY OF SEQ-LENGTHS L AND SPATIO-TEMPORAL METHODS. WE COMPARE: (I) RECURRENT-TE (NON-DEFORMABLE TRANSFORMER ENCODER WITH RECURRENCE), (II) DTE+TT (DTE WITH A SEPARATE TEMPORAL TRANSFORMER), (III) DTE ONLY (OURS WITHOUT RECURRENCE), AND (IV) RECURRENT-DTE (OURS).

L	Spatio-Temp. Method	Oxford-Hard		NuScenes		Resource Usage	
		R@5 ↑	R@5 ↑	Mem(MB) ↓	Time(s) ↓	Mem(MB) ↓	Time(s) ↓
1	Recurrent-TE	0.4776	0.1173	98.15	0.0120		
	DTE + TT	0.7368	0.5106	106.02	0.0122		
	DTE Only (non-recurrent)	0.7306	<u>0.5283</u>	88.71	0.0111		
	Recurrent-DTE (Ours)	<u>0.7341</u>	0.6224	88.71	0.0115		
3	Recurrent-TE	0.4552	0.1303	<u>136.75</u>	0.0135		
	DTE + TT	<u>0.7384</u>	0.4764	152.03	0.0177		
	DTE Only (non-recurrent)	0.7255	0.4898	134.39	0.0126		
	Recurrent-DTE (Ours)	0.7549	0.6681	134.39	0.0128		
5	Recurrent-TE	0.4085	0.1111	182.75	0.0181		
	DTE + TT	<u>0.7341</u>	0.4677	198.16	0.0267		
	DTE Only (non-recurrent)	0.7247	0.4693	180.39	0.0176		
	Recurrent-DTE (Ours)	0.7706	0.7039	180.39	0.0178		

Disclaimer: Recurrent-TE and the DTE + TT ablation baselines were integrated with minimal tuning.

usage (152.03MB vs. 134.39MB). These results demonstrate that our recurrent-DTE is efficient and effective at spatio-temporal modeling.

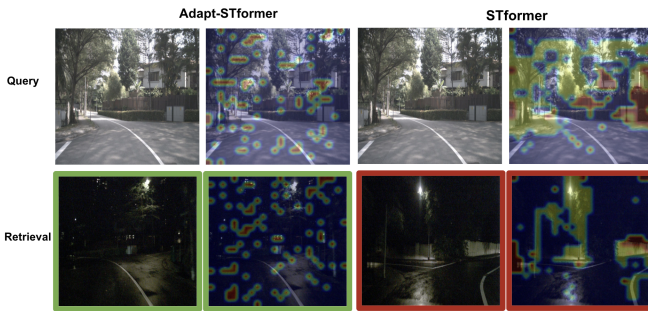
DTE Module: Finally, replacing our deformable transformer encoder with a non-deformable variant (Recurrent-TE baseline) degrades both performance and efficiency. As shown in Table V, the deformable design improves recall by +29.4% on Oxford-Hard ($L = 5$: 0.7706 vs. 0.4085) and +492% on NuScenes ($L = 5$: 0.7039 vs. 0.1111), while simultaneously lowering memory (180.39MB vs. 182.75MB) and inference time (0.0178s vs. 0.0181s).

E. Qualitative Results

Based on the ablation results, DTE is effective at capturing spatial features. Figure 3 shows NuScenes examples where our model retrieves correctly while STformer fails. In both day and night frames, STformer produces smooth, concen-



(a) NuScenes Example 1



(b) NuScenes Example 2

Fig. 3: Qualitative comparison of attention maps between our method and STformer on NuScenes. STformer fails in these cases, whereas our method succeeds in VPR matching. In the attention maps, blue denotes low-focus regions and yellow to red gradient denotes high-focus regions by the respective models.

trated activations over only a few regions. By contrast, our model displays scattered high-activation patches across the entire frame. This difference, we theorize, arises from the type of attention used. Standard attention, used by STformer, computes attention between every token pair, producing blob-shaped activations around globally salient regions. In contrast, deformable attention, used by our method, learns a small set of sparse offsets that jump directly to features relative to the query token, yielding scattered activations. Under poor lighting, many features are weak, making it crucial to capture any available geometric cues scattered across the scene. Under poor lighting, it is essential to exploit sparse geometric cues across the scene rather than depend on regions salient only under good illumination.

F. Refinement across modules

Figure 4 illustrates the progressive refinement of features across the stages of Adapt-STformer when processing a lighting-distorted input (a). At the encoder stage (b), distortions are partially reduced and an initial set of features is extracted, though these can be unreliable, often emphasizing small wall patches susceptible to perceptual aliasing and transient objects such as vehicles. Following DTE refinement (c), the model attends to a broader and more discriminative set of VPR-relevant features, with greater emphasis on stable structural cues (e.g., sidewalks and roadside vegetation)

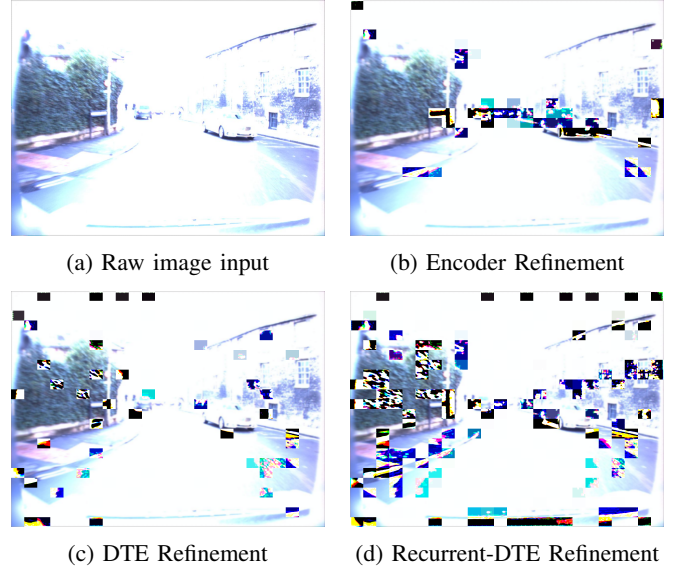


Fig. 4: **Feature Refinement Across Adapt-STformer’s Modules.** Subfigures (b)–(d) are snapshots of the model’s attention during inferencing stages, indicated by pixelated areas.

and reduced focus on transient objects. At the Recurrent-DTE stage (d), cross-frame interactions are incorporated, reinforcing features that persist temporally. Relative to (c), the resulting attention is more concentrated on salient and persistent VPR cues such as road boundaries, buildings, and vegetation.

G. Comparison with SOTA VPR Methods

Though Adapt-STformer outperforms the Seq-VPR baselines without a foundation model image encoder, its performance is yet to be compared to SOTA VPR methods. We benchmark Adapt-STformer against CricaVPR [20] and CaseNet [13]. We also include STformer in this analysis as it’s the 2nd-strongest SeqVPR baseline and the closest architectural counterpart to our method. Besides computing recall conventionally (ie. with unlimited time budget), we analyze the real-world performance of all models by imposing inferencing time constraints.

We continuously stream queries at 36 frames per second (FPS)—matching the reported Tesla vehicle surround-camera rate. If a successful prediction arrives after the next query, it will not count as a successful recall under the Recall@K metric. In Table VI, we report (i) conventional Recall@5, (ii) the percentage of queries processed on-time OT%, and (iii) Recall@5 computed over the on-time subset. To comprehensively understand the performance of Adapt-STformer and SOTA VPR methods in efficiency-critical environments, we also plot Recall@5 across FPS values from 20 to 60 in Figure 5, fully covering the typical driver assistance FPS range [30].

Recall under Time Constraints: At 36fps, only Adapt-STformer achieves OT% = 100%, so recall remains equal to its conventional R@5 across all datasets (Table VI).

TABLE VI

PERFORMANCE OF ADAPT-STFORMER AND SOTA VPR METHODS. WE COMPUTE THE RECALL@5 (R@5), RECALL@5 GIVEN ON-TIME PROCESSING OF QUERIES AT 36 FPS (R@5-36FPS), THE PERCENTAGE OF QUERIES PROCESSED ON-TIME (OT%), AND RESOURCE USAGE.

Method	Nordland		Oxford-Easy		Oxford-Hard		NuScenes		OT% \uparrow	Resource Usage		
	R@5 \uparrow	R@5-36FPS \uparrow		GFLOPs \downarrow	Mem (MB) \downarrow	Time (s) \downarrow						
CricaVPR	0.9900	0.4953	0.9803	0.4891	0.8276	0.3822	0.8626	0.8622	68.36	138.62	517.77	0.029
CaseVPR	0.9850	0.3280	0.9882	0.3280	0.8492	0.2549	0.8642	0.2081	33.34	503.62	641.33	0.070
STFormer	0.9947	<u>0.5153</u>	0.9372	<u>0.9136</u>	0.6453	0.3000	0.5319	0.5154	<u>84.78</u>	<u>127.74</u>	<u>276.55</u>	<u>0.028</u>
Ours	<u>0.9923</u>	0.9923	0.9618	0.9618	0.7659	0.7659	0.7031	<u>0.7031</u>	100.0	102.00	180.39	0.018

Note: We use public checkpoints for CaseVPR (no training code released) and CricaVPR (incompatible training procedure). Note that both methods were trained on far larger datasets than ours.

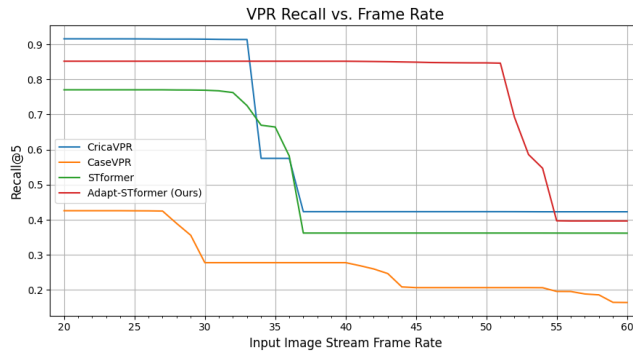


Fig. 5: **VPR Performance Under Time Constraints.** We analyze the impacts of changing inference time constraints on the performance of Adapt-STformer and other SOTA VPR methods by streaming queries from 20 FPS to 60 FPS.

Against STFormer (the next-fastest), our recall is higher by +47.7% on Nordland (0.9923 vs. 0.5153), +4.8% on Oxford-Easy, +46.6% on Oxford-Hard, and +18.8% on NuScenes (0.7031 vs. 0.5154). Although DINOv2-based CaseVPR and CricaVPR often lead in conventional R@5, their lower OT% (33.34% and 68.36%) causes large drops in recall under time constraints; an exception is NuScenes, where CricaVPR remains best at 0.8622. Overall, Adapt-STformer sustains high recall under time pressure while using the fewest GFLOPs, the least memory, and the lowest per-sequence inference latency.

Qualitative Trajectory Mappings: In Figure 6, we plot all VPR models’ predicted locations of queries on Oxford-Easy. Queries are color-coded according to their index value. Qualitatively, our trajectories are the smoothest and densest, closely tracking ground truth; quantitatively, the latency-adjusted metrics explain this advantage. Although simpler methods (JIST/SeqNet/SeqVLAD) have fast inference speeds (Table III), their lower performance yields fragmented maps, where notable segments of the dataset couldn’t be corrected predicted. Conversely, CricaVPR and CaseNet produce accurate predictions but at slower speeds, resulting in many omitted queries and likewise fragmented trajectories despite high conventional recall.

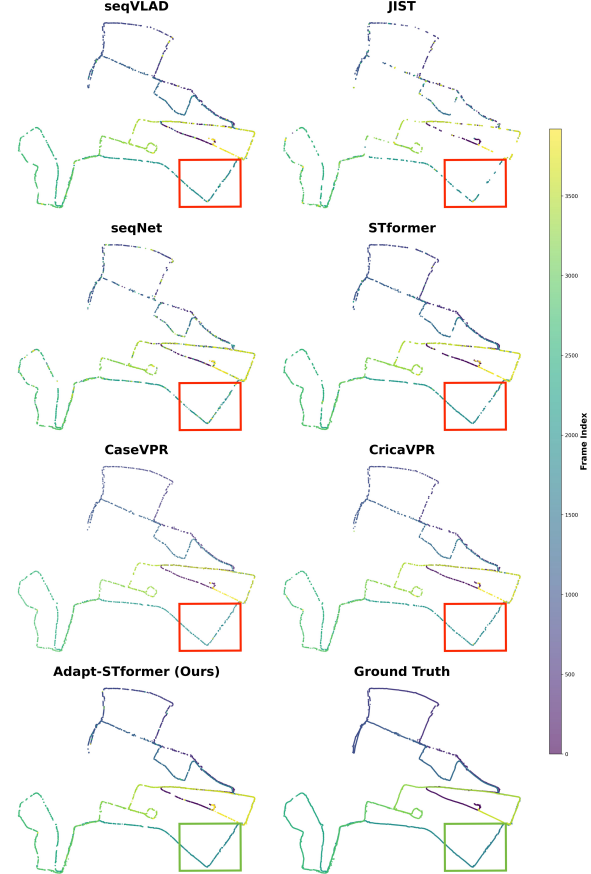


Fig. 6: Mapping results on Oxford-Easy. Predicted trajectories are color-coded by frame index. Compared to baselines, Adapt-STformer aligns most closely with the Ground Truth, consistent with its high latency-adjusted recall (Table VI). Green highlights mark better alignments by our method, while red indicates baseline errors

Practical implication: When real-time constraints apply, a lighter backbone paired with an efficient spatio-temporal module yields better timely recognition – higher OT% and higher recall under time constraints – while also reducing memory footprint and inference time. This makes our approach a stronger choice for latency-critical VPR applications, even against more powerful alternatives.

III. LIMITATION

We did not investigate the effects of using other image encoder backbones, most notably DINOv2 [14], on Adapt-STformer’s performance. Though we are outperformed by SOTA VPR methods in traditional settings, we drastically reduce inference time and memory usage.

IV. CONCLUSION

We present Adapt-STformer, a Seq-VPR framework that balances flexibility, efficiency, and performance. Central to our design is the Recurrent-DTE module, which unifies spatial and temporal modeling. This approach improves computational efficiency, adapts to variable seq-lengths, and constructs discriminative sequential VPR descriptors. Adapt-STformer thus establishes a foundation for future research on efficient, flexible and high performing Seq-VPR systems.

REFERENCES

- [1] S. Garg and M. Milford, “Seqnet: Learning descriptors for sequence-based hierarchical place recognition,” *IEEE Robot. Automat. Lett.*, vol. 6, no. 3, pp. 4305–4312, 2021. 1, 2, 4
- [2] Z. Li, W. Wang, H. Li, E. Xie, C. Sima, T. Lu, Q. Yu, and J. Dai, “Bevformer: Learning bird’s-eye-view representation from multi-camera images via spatiotemporal transformers,” in *Computer Vision – ECCV 2022*, ser. Lecture Notes in Computer Science, vol. 13669. Springer, 2022, pp. 1–18. 1, 2, 3
- [3] R. Mereu, G. Trivigno, G. Berton, C. Masone, and B. Caputo, “Learning sequential descriptors for sequence-based visual place recognition,” *IEEE Robot. Automat. Lett.*, vol. 7, no. 4, pp. 10383–10390, 2022. 1, 2, 3, 4
- [4] G. Berton, G. Trivigno, B. Caputo, and C. Masone, “Jist: Joint image and sequence training for sequential visual place recognition,” *IEEE Robot. Automat. Lett.*, vol. 9, no. 2, pp. 1310–1317, 2024. 1, 2, 3, 4
- [5] G. Bertasius, H. Wang, and L. Torresani, “Is space-time attention all you need for video understanding?” in *Proc. 38th Int. Conf. Mach. Learn. (ICML)*, ser. Proceedings of Machine Learning Research, vol. 139, 2021, pp. 813–824. 1
- [6] C. Feichtenhofer, A. Pinz, and R. P. Wildes, “Spatiotemporal multiplier networks for video action recognition,” in *Proc. IEEE Conf. Comput. Vis. Pattern Recognit. (CVPR)*, 2017, pp. 4769–4778. 1, 2
- [7] A. Cherian, J. Wang, C. Hori, and T. K. Marks, “Spatio-temporal ranked-attention networks for video captioning,” in *2020 IEEE Winter Conf. Appl. Comput. Vis. (WACV)*, 2020, pp. 1606–1615. 1, 2
- [8] J. Zhao, F. Zhang, Y. Cai, G. Tian, W. Mu, C. Ye, and T. Feng, “Learning sequence descriptor based on spatio-temporal attention for visual place recognition,” *IEEE Robot. Automat. Lett.*, vol. 9, no. 3, pp. 2351–2358, 2024. 1, 2, 3, 4, 5
- [9] R. M. Schmidt, “Recurrent neural networks (rnns): A gentle introduction and overview,” *arXiv preprint arXiv:1912.05911*, 2019. 1
- [10] J. M. Fácil, D. Olid, L. Montesano, and J. Civera, “Condition-invariant multi-view place recognition,” *arXiv preprint arXiv:1902.09516*, 2019. 1
- [11] M. J. Milford and G. F. Wyeth, “Seqslam: Visual route-based navigation for sunny summer days and stormy winter nights,” in *Proc. IEEE Int. Conf. Robot. Automat. (ICRA)*, 2012, pp. 1643–1649. 2
- [12] R. Arandjelović, P. Gronat, A. Torii, T. Pajdla, and J. Sivic, “Netvlad: Cnn architecture for weakly supervised place recognition,” in *Proc. IEEE Conf. Comput. Vis. Pattern Recognit. (CVPR)*, 2016, pp. 5297–5307. 2, 4
- [13] H. Li, G. Peng, J. Zhang, M. Wen, Y. Ma, and D. Wang, “Casevpr: Correlation-aware sequential embedding for sequence-to-frame visual place recognition,” *IEEE Robot. Automat. Lett.*, vol. 10, no. 4, pp. 3430–3437, 2025. 2, 4, 5, 6
- [14] M. Oquab, T. Darcet, T. Moutakanni, H. Vo, M. Szafraniec, V. Khalidov, P. Fernandez, D. Haziza, F. Massa, A. El-Nouby, M. Assran, N. Ballas, W. Galuba, R. Howes, P.-Y. Huang, S.-W. Li, I. Misra, M. Rabbat, V. Sharma, G. Synnaeve, H. Xu, H. Jégou, J. Mairal, P. Labatut, A. Joulin, and P. Bojanowski, “Dinov2: Learning robust visual features without supervision,” *arXiv preprint arXiv:2304.07193*, 2023. 2, 8
- [15] X. Zhu, W. Su, L. Lu, B. Li, X. Wang, and J. Dai, “Deformable DETR: Deformable transformers for end-to-end object detection,” in *Int. Conf. Learn. Representations (ICLR)*, 2021. 2, 3
- [16] X. Xu, Y. Jiao, S. Lu, X. Ding, R. Xiong, and Y. Wang, “Leveraging bev representation for 360-degree visual place recognition,” *arXiv preprint arXiv:2305.13814*, 2023. 2
- [17] F. Ge, Y. Zhang, S. Shen, Y. Wang, W. Hu, and J. Gao, “Bev²pr: Bev-enhanced visual place recognition with structural cues,” in *Proc. 2024 IEEE/RSJ Int. Conf. Intell. Robots Syst. (IROS)*, 2024, pp. 13274–13281. 2, 4
- [18] H. Caesar, V. Bankiti, A. H. Lang, S. Vora, V. E. Liong, Q. Xu, A. Krishnan, Y. Pan, G. Baldan, and O. Beijbom, “nuscenes: A multimodal dataset for autonomous driving,” in *Proc. IEEE/CVF Conf. Comput. Vis. Pattern Recognit. (CVPR)*, 2020, pp. 11618–11628. 2, 4
- [19] K. He, X. Zhang, S. Ren, and J. Sun, “Deep residual learning for image recognition,” in *Proc. IEEE Conf. Comput. Vis. Pattern Recognit. (CVPR)*, June 2016. 2
- [20] F. Lu, X. Lan, L. Zhang, D. Jiang, Y. Wang, and C. Yuan, “Cricavpr: Cross-image correlation-aware representation learning for visual place recognition,” in *Proc. IEEE/CVF Conf. Comput. Vis. Pattern Recognit. (CVPR)*, June 2024. 2, 4, 6
- [21] A. Hassani, S. Walton, N. Shah, A. Abuduweili, J. Li, and H. Shi, “Escaping the big data paradigm with compact transformers,” *arXiv preprint arXiv:2104.05704*, 2021. 2, 4
- [22] A. Dosovitskiy, L. Beyer, A. Kolesnikov, D. Weissenborn, X. Zhai, T. Unterthiner, M. Dehghani, M. Minderer, G. Heigold, S. Gelly, J. Uszkoreit, and N. Houlsby, “An image is worth 16×16 words: Transformers for image recognition at scale,” in *Proc. 9th Int. Conf. Learn. Representations (ICLR)*, 2021. 2
- [23] N. Sünderhauf, P. Neubert, and P. Protzel, “Are we there yet? challenging seqslam on a 3000 km journey across all four seasons,” in *Proc. IEEE ICRA Workshop on Long-Term Autonomy*, 2013. 4
- [24] W. Maddern, G. Pascoe, C. Linegar, and P. Newman, “1 year, 1000km: The oxford robotcar dataset,” *Int. J. of Robotics Research*, vol. 36, no. 1, pp. 3–15, 2017. 4
- [25] W. Maddern, G. Pascoe, M. Gadd, D. Barnes, B. Yeomans, and P. Newman, “Real-time kinematic ground truth for the oxford robotcar dataset,” *arXiv preprint arXiv:2002.10152*, 2020. 4
- [26] D. P. Kingma and J. Ba, “Adam: A method for stochastic optimization,” *arXiv preprint arXiv:1412.6980*, 2014. 4
- [27] H. Jégou and O. Chum, “Negative evidences and co-occurrences in image retrieval: The benefit of pca and whitening,” in *Proc. European Conf. Comput. Vis. (ECCV)*, 2012. 4
- [28] A. Paszke, S. Gross, F. Massa, A. Lerer, J. Bradbury, G. Chanan, T. Killeen, Z. Lin, N. Gimelshein, L. Antiga, A. Desmaison, A. Kopf, E. Yang, Z. DeVito, M. Raison, A. Tejani, S. Chilamkurthy, B. Steiner, L. Fang, J. Bai, and S. Chintala, “Pytorch: An imperative style, high-performance deep learning library,” in *Advances in Neural Inf. Process. Syst. 32 (NeurIPS 2019)*, 2019, pp. 8024–8035. 4
- [29] C. Malone, A. Vora, T. Peynot, and M. Milford, “Dynamically modulating visual place recognition sequence length for minimum acceptable performance scenarios,” in *Proc. 2024 IEEE/RSJ Int. Conf. Intell. Robots Syst. (IROS)*, 2024, pp. 3340–3347. 5
- [30] D. Gehrig and D. Scaramuzza, “Low-latency automotive vision with event cameras,” *Sci. Robot.*, May 2024. 6